Chinese Chemical Letters 32 (2021) 3954–3961

Contents lists available at ScienceDirect

Chinese Chemical Letters

journal homepage: www.elsevier.com/locate/cclet

Communication

Dual-labeled visual tracer system for topical drug delivery by nanoparticle-triggered P-glycoprotein silencing

Jushan Gao[a,1], Shanbo Ma[b,1], Xinxin Zhao[a], Jinpeng Wen[a], Datao Hu[a], Xiaoye Zhao[a], Xiaopeng Shi[b,*], Ke Wang[a,*]

[a] School of Pharmacy, Health Science Center, Xi'an Jiaotong University, Xi'an 710061, China
[b] Department of Pharmacy, Xijing Hospital, Fourth Military Medical University, Xi'an 710032, China

ARTICLE INFO

Article history:
Received 1 April 2021
Revised 10 June 2021
Accepted 14 June 2021
Available online 24 June 2021

Keywords:
Transdermal delivery
Nanoparticle
Stratum corneum
Dermis
Transdermal enhancer

ABSTRACT

Using nanoparticle-based drug delivery systems as enhancers is a robust strategy for transdermal delivery; however, the mechanisms by which these systems promote transdermal penetration are still unclear. Here, we fabricated a dual-labeled nano drug delivery system that allows discrete visualization of both the drug and the nanoparticle carrier. To comprehensively examine its potential mechanism, we investigated its effects on human epidermal keratinocyte HaCaT cells, including changes in cell membrane potential, intracellular Ca^{2+} concentration, and Ca^{2+}-ATPase activity. P-glycoprotein (P-gp) expression in nanoparticle-treated human dermal microvascular endothelial cells was detected by western blotting and immunofluorescence. Furthermore, the transdermal absorption and biodistribution of the dual-labeled nanoparticles were deeply investigated by skin permeability study *in vitro* and *in vivo* using fluorescence microscopy and *in vivo* imaging, respectively. In addition to reducing membrane potential, increasing the intracellular Ca^{2+} concentration, and decreasing Ca^{2+}-ATPase activity, our results indicate that the dual-labeled nanoparticles can downregulate P-gp to promote transdermal absorption. Fluorescence and *in vivo* imaging visually demonstrated that the nanoparticle delivery system penetrated into the dermis through the stratum corneum. All these results indicate that this dual-labeled nano delivery system provides a new method for future in-depth visual explorations of transdermal drug delivery mechanisms.

A dual-labeled nanoparticle drug delivery system was developed for topical drug delivery by nanoparticle-triggered P-glycoprotein (P-gp) silencing, which can simultaneously track a drug and its carrier to systematically and vividly observe the transdermal process.

Polymer nanoparticles are the most advanced drug delivery system developed and have received increasing attention over the past few decades [1,2]. With a small size, targeted effect, and functional surface, it can efficiently increase drug stability, enhance therapeutic effect and decrease toxic side effects [3]. In recent years, polymer nanoparticles were gradually used as percutaneous permeation enhancers, opening a new delivery avenue for drugs [4,5]. Compared with simple chemical transdermal enhancers, polymeric nanoparticles have been widely reported it has more significant permeation effects, less skin irritation or toxicity [6–8]. Generally, chemical enhancers play their roles through rearranging the lipids barrier, protein distribution, or dense structure of keratinocytes [9]. While the specific mechanism of polymeric nanoparticles that promoting drug penetration into human skin is still unknown.

Current chemical transdermal enhancers mainly include terpenes, azone, volatile oils, glycols, and ethanol, *etc*. Their mechanistic investigations have mainly focused on topical effects on stratum corneum cells [10]. These enhancers could regulate the surface potential, Ca^{2+}, and Ca^{2+}-ATPase concentration of keratinocytes to reduce skin resistance and increase transdermal delivery content of the drug [11–14]. However, whether nanoparticle enhancers play the same role in stratum corneum cells remains unclear. In addition, along with the keratinocyte layer, dermal cells are also an unavoidable conduit for drug delivery into the blood circulation [15]. Therefore, the effects of nanoparticles on dermal cells also cannot be ignored. P-gp, a product of the multidrug resistance 1 gene (MDR-1), is a well-known multidrug efflux pump that mainly functions in excreting extraneous substances from cells [16], and when highly expressed, enhances the multidrug resistance of tumor cells

* Corresponding authors.
E-mail addresses: shixiaopeng775471@163.com (X. Shi), perpetual1003@mail.xjtu.edu.cn (K. Wang).
[1] These authors contributed equally to this work.

https://doi.org/10.1016/j.cclet.2021.06.040
1001-8417/

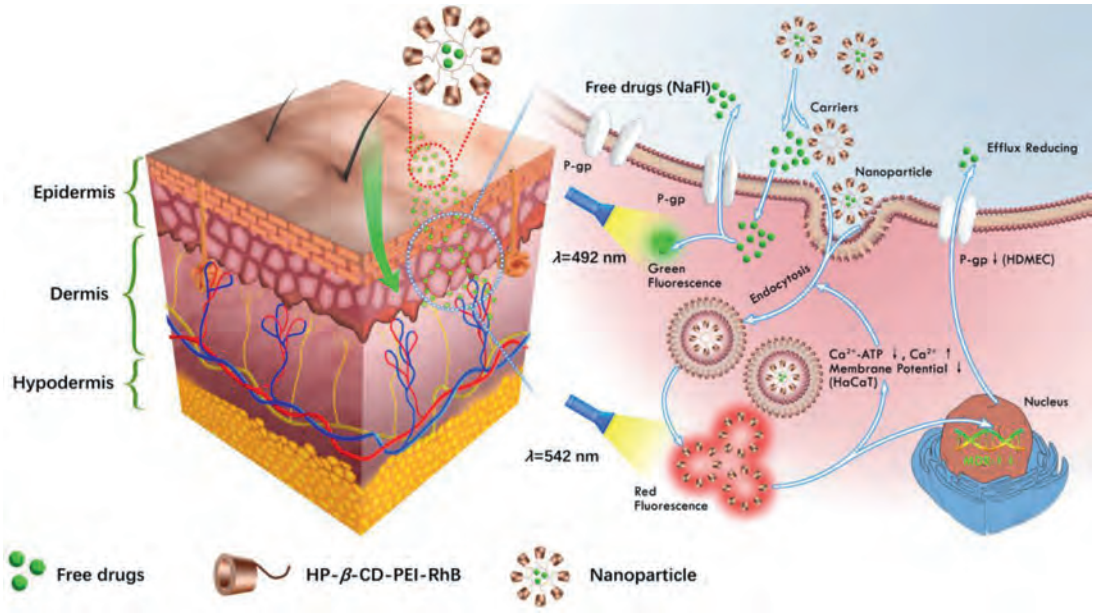

Scheme 1. The transcutaneous process and its mechanism of the nanoparticle drug delivery system.

[17,18]. In recent years, the effects of P-gp on cutaneous absorption have piqued the interest of many researchers. It has been widely reported that P-gp could be involved in the transdermal penetration and distribution of various drugs. Hashimoto *et al.* found that P-gp expression in the skin contributed to the transdermal absorption of some corticosteroids *in vivo* [19,20]. Giacone *et al.* reported that a P-gp inhibitor-loaded nanoemulsion reduced the dermal penetration of the antitumor drug paclitaxel [21]. Fujita *et al.* found that P-gp is expressed at low levels in keratinocytes and fibroblasts, but is highly expressed in skin microvascular endothelial cells [22]. However, whether nanoparticle carriers can regulate dermal P-gp expression to influence the cutaneous effects is not fully understood. Therefore, we used human dermal microvascular endothelial cells (HDMECs) to explore the influence of a nanoparticle enhancer on P-gp expression.

Except for the interactions of polymeric nanoparticles with specific cells or proteins, the complex skin penetration process is also an urgent challenge. Thus, developing a novel strategy for mechanism investigation involved in the penetration process would be contributed to transdermal and topical drug delivery. The current majority of studies have tracked drug delivery unilaterally by replacing the model drug with fluorescent dyes like coumarin 6, rhodamine B (RhB), fluorescein isothiocyanate (FITC), without simultaneously tracking the nanocarriers [23–25]. These delivery systems were unable to determine whether the drug enters the body alone or with the carrier during the delivery process, or when and where the nanoparticle drug delivery system disintegrated. Therefore, we aimed to design a dual-labeled fluorescent nano-drug delivery system that would enable visual monitoring of both the drug and the carrier material. Depending on the different excitation wavelengths design, the status of the nanoparticle drug delivery system can be visually presented during transcutaneous drug delivery.

Herein, we developed a dual-labeled nanoparticle drug delivery system that can simultaneously track a drug and its carrier and used fluorescence imaging to systematically and vividly observe the transdermal process. In our previous works, a novel 2-hydroxypropyl-β-cyclodextrin (HP-β-CD)-polyethyleneimine (PEI) cationic nanoparticle has been synthesized [26,27]. In this work, we constructed a dual labeled visual tracer system by using HP-β-CD-PEI grafted with RhB as a nanoparticle carrier, and sodium fluorescein (NaFl) as a model drug. The different excitation and emission wavelengths of RhB and NaFl allow visualization of both components during transdermal drug delivery (Scheme 1). Furthermore, we also examined the surface potential, Ca^{2+} concentration, and Ca^{2+}-ATPase activity of HaCaT cells treated with the nanoparticles. To study the effects of the dual-labeled nano-drug delivery system on P-gp expression in HDMECs, P-gp mRNA was detected by quantitative real-time polymerase chain reaction (qPCR), and P-gp protein was detected by western blotting. In addition, to comprehensively analyze the mechanism of transdermal drug delivery, *in vitro* and *in vivo* skin permeability was conducted on Sprague Dawley rats using fluorescence microscopic imaging and the small animal live imaging system (IVIS), respectively. This new analytical method of observing transcutaneous drug delivery could provide novel strategies to enhance skin penetration and accelerate the development of transdermal drug delivery systems.

The HP-β-CD-PEI was prepared as previously described. The PEI was grafted with HP-β-CD through the CDI-mediated coupling reaction. Then the RhB was crosslinked with HP-β-CD-PEI by amide reaction to yield HP-β-CD-PEI-RhB. In presence of strong electrostatic interaction, NaFl and HP-β-CD-PEI-RhB self-assembled into the nanoparticle delivery system. In Figs. 1A and B, it could be observed that the delivery system had a quite small size, spherical appearance, and smooth surface**.** Its hydrodynamic size was about 10 nm, which was consistent with the results of TEM **(**Fig. 1C). Meanwhile, as we expected, its corresponding zeta potential value was approximately 15 mV (Fig. 1D). It suggested that the negatively charged NaFl was successfully encapsulated in positive HP-β-CD-PEI-RhB nanoparticles.

The successful formation of the nanoparticle delivery system was also confirmed by X-ray diffraction (XRD). As presented in Fig. 1E, XRD patterns of the HP-β-CD-PEI nanoparticle, NaFl, HP-β-CD-PEI/NaFl mixture, and NaFl-loaded nanoparticles are determined from $2\theta = 10°$ to 100° HP-β-CD-PEI-RhB nanoparticles have a broad peak at 2θ angles of 15–25° which attributed to the amorphous character of the HP-β-CD molecular. Multiple sharp peaks at $2\theta = 15–55°$ represented the crystal structure of NaFl. These peaks could be observed in HP-β-CD-PEI-RhB/NaFl physical mixture state, while they disappeared in self-assembled HP-β-CD-PEI-RhB/NaFl nanoparticle delivery system. It indicated that NaFl was

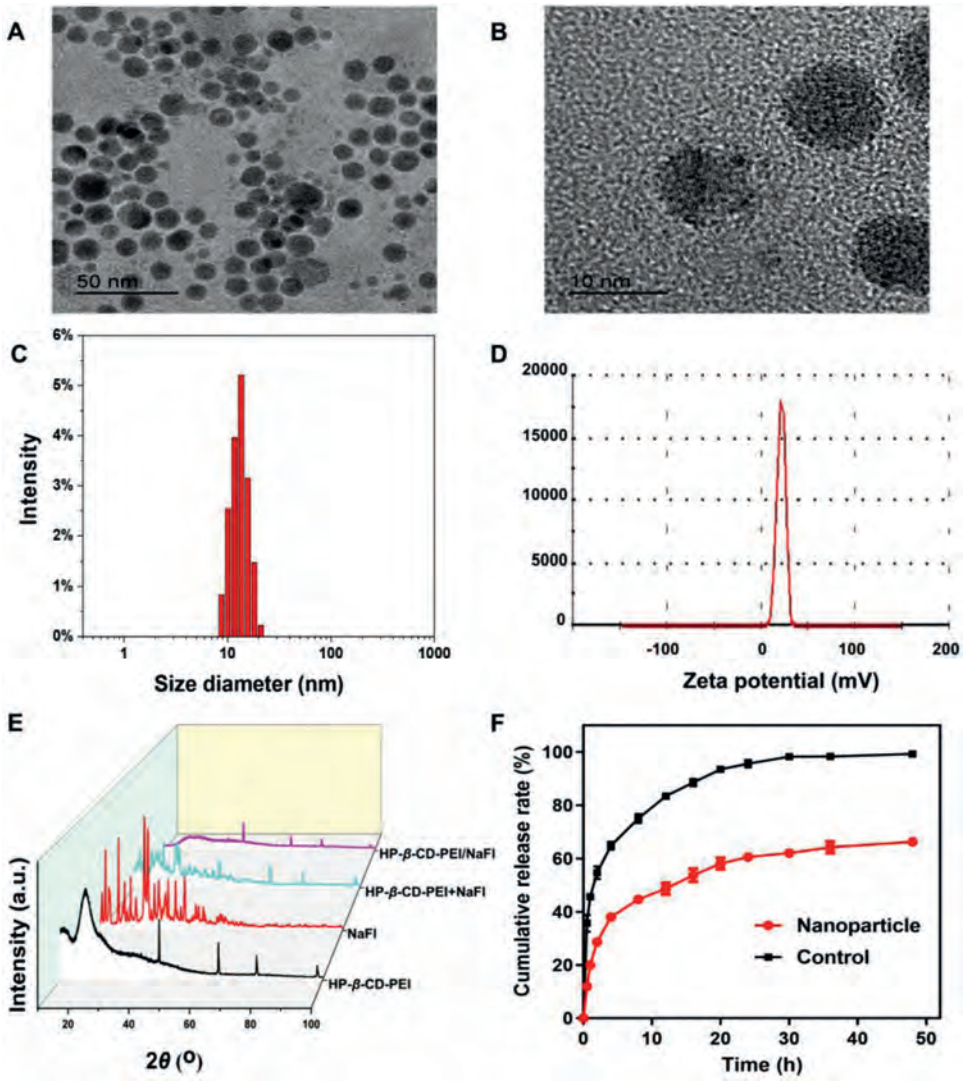

Fig. 1. The characterization and *in vitro* drug release of nanoparticle delivery system. (A) The transmission electron microscopy (TEM) image of nanoparticles, scale bar: 50 nm. (B) The TEM image of nanoparticles, scale bar: 10 nm. The dynamic light scattering (DLS) size (C) and zeta potential (D) of nanoparticle drug delivery system. (E) X-ray powder diffraction pattern of HP-β-CD-PEI nanoparticle, NaFl, HP-β-CD-PEI and NaFl mixture, NaFl-loaded nanoparticle, respectively. (F) *In vitro* release behavior of NaFl from nanoparticles. Data are presented as mean ± SEM ($n = 3$).

homogeneously incorporated into the HP-β-CD-PEI-RhB nanoparticles under strong electrostatic interaction.

The encapsulation and release behavior of the HP-β-CD-PEI-RhB/NaFl nanoparticle delivery system was investigated and quantified by ultraviolet-visible (UV–vis) spectroscopy analysis. The drug loading content of the nanoparticles was 36.9% and their encapsulation efficiency was 12.3%. Meanwhile, the *in vitro* cumulative release profile of NaFl from nanoparticles was measured in PBS (pH 7.4, 37 °C). Fig. 1F showed that NaFl solution without nanoparticles exhibited burst release of approximately 40% in early, and release account was close to 100% at 24 h. While NaFl encapsulated in the nanoparticles displayed a dual-kinetic release curve. It had a burst release initially and later followed by slow sustained release. This result was attributed to the high solubility of nanoparticles in release media and the NaFl deposited near to the surface of nanoparticles [28]. The NaFl near to the surface solved quickly resulting in an initial burst release. In contrast, the drug NaFl entrapped in the core of nanoparticles showed sustained release due to the long diffuse pathway and the hydrophobic cavity of the HP-β-CD shell [29]. The hydrophobic structure present on the surface could slow down the penetration of solution media to modulate release speed [30]. Therefore, the nanoparticle could stably and sustained release the drug NaFl over a relatively long period, which could greatly decrease toxicity from the burst release and prolonged the therapeutic time [31,32].

As we know, the stratum corneum was the major barrier for transdermal penetration. Only when crossing through the stratum corneum and significantly accumulating in the dermal layer, nanoparticles could effectively deliver the drug to blood circulation and therapy diseases [33]. In order to check the penetration efficiency of nanoparticle drug delivery system, *In vitro* permeation study was investigated using Franz diffusion cells. When the isolated skins were treated with normal saline (NS; control), PEI, HP-β-CD and HP-β-CD-PEI-RhB nanoparticle for 48 h, the cumulative penetration amount of NaFl was determined at predetermined time points. All animal experimental procedures were conducted in conformity with protocols approved by the Ethical Committee of Xi'an Jiaotong University (permit No. XJTU 2019–003). As presented in Fig. 2A, the cumulative release amount of NaFl from HP-β-CD-PEI-RhB nanoparticle increased steadily with time. After 48 h, the cumulative release amount of NaFl from HP-β-CD-PEI-RhB nanoparticles was 34-fold that from NS ($P < 0.001$).

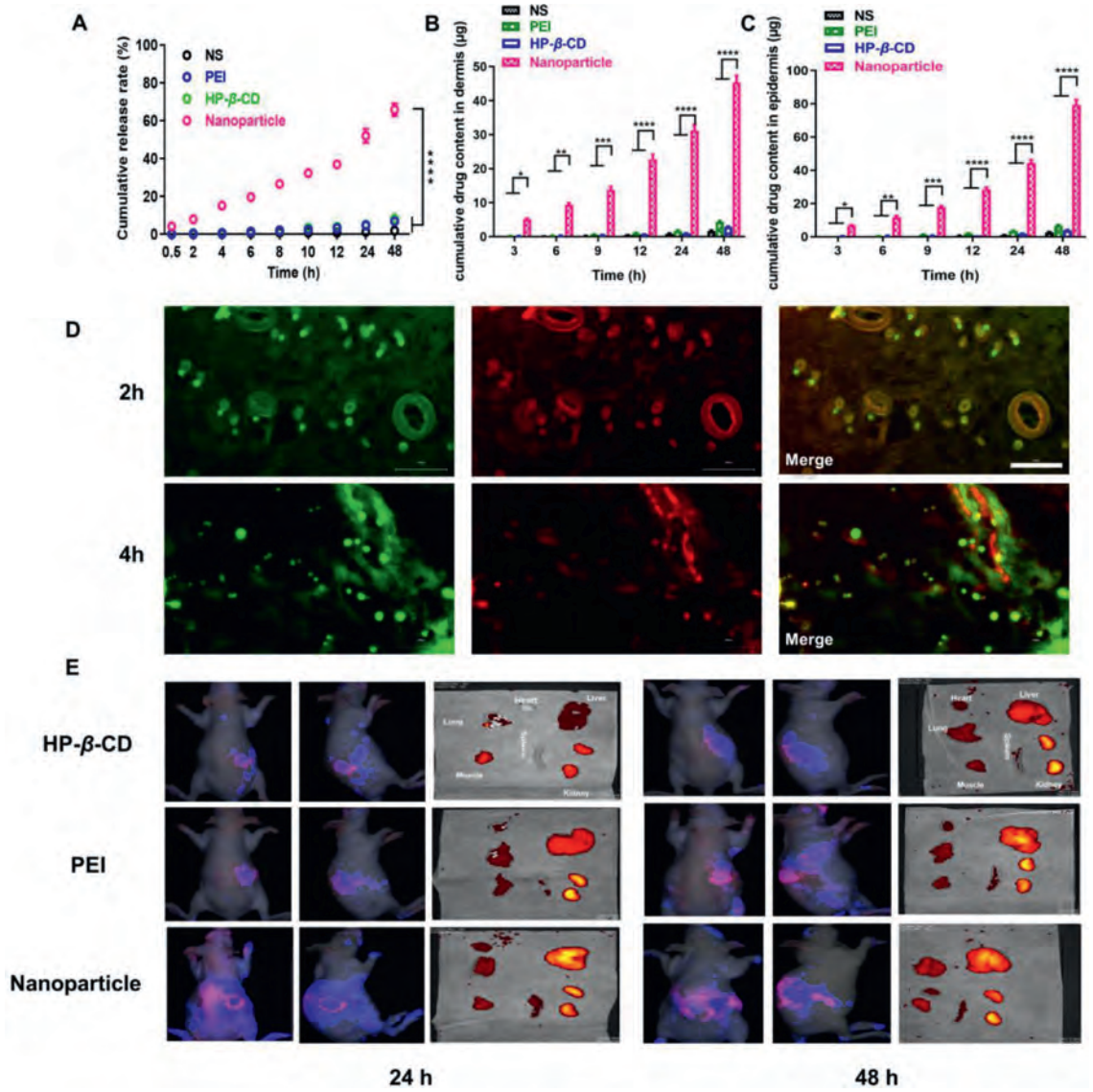

Fig. 2. *In vitro* and *vivo* permeation assay. (A) *In vitro* cumulative transcutaneous permeation profiles of the drug through the excised rat skins. Data expressed as mean ± SD ($n = 5$). The cumulative amount of nanoparticles in the epidermis (B) and dermis (C) treated with normal saline (NS), PEI, HP-β-CD, and nanoparticles after 3, 6, 9, 12, 24, and 48 h, respectively ($n = 6$). (D) *In vitro* fluorescent images of skin after treated with nanoparticles for 2 h and 4 h, respectively (green stand for the drug NaFl, red stand for nanoparticles). Scale bar: 100 μm. (E) *In vivo* fluorescence images at 24 h and 48 h. After treated with the PEI, HP-β-CD, and nanoparticles (40 mg/mL per rat) for 24 h and 48 h by transdermal administration, the rats were anesthetized for *in vivo* imaging. Then, they were euthanized, and their muscles and all kinds of organs like heart, liver, spleen, lung, and kidney were excised for *ex vivo* imaging. In both cases, the excitation wavelength was 540 nm, with emission at 625 nm. Data are presented as mean ± SEM ($n = 6$). $^{*}P < 0.05$, $^{**}P < 0.01$, $^{***}P < 0.001$ and $^{****}P < 0.0001$.

Conversely, in the PEI and HP-β-CD samples, the amount of NaFl slightly increased after 48 h of treatment. It suggested that the HP-β-CD-PEI-RhB nanoparticles had excellent penetration enhancing effects.

To further quantitively observe the distribution of nanoparticles in the epidermis and dermis layer, *in vivo* skin permeation assays were performed on Sprague Dawley rats [26]. The obtained distribution results were consistent with *in vitro* permeation study (Figs. 2B and C). The cumulative drug content penetrating the dermis was 25-fold higher with HP-β-CD-PEI-RhB nanoparticles than NS at 48 h ($P < 0.001$). Similarly, in the epidermis, we got an alike result that the penetration amount of NS, PEI, and HP-β-CD was significantly lower than nanoparticles. These results confirmed that HP-β-CD-PEI-RhB nanoparticles had high transcutaneous penetration effects for the hydrophilic NaFl and it could effectively traverse the intact epidermis and penetrate the dermis. This good performance could be due to its small size, large specific surface areas, and high density of superficial positive charges [34,35]. As mentioned above, the HP-β-CD-PEI-RhB nanoparticle delivery system had a mean size of ~10 nm, which could efficiently enhance cellular uptake. Besides, strong electrostatic interactions between the nanoparticles and cells could improve cytomembrane adherence and induce fluidity in the lipid bilayer [36,37]. It could greatly decrease the compact structure of the stratum corneum, further contributing to transcutaneous penetration.

To visually observe and evaluate the dynamic transdermal process of the nanoparticles, the real-time penetration through skin of HP-β-CD-PEI-RhB nanoparticles delivery system at different time intervals was recorded using a fluorescence microscope (Olympus CX41, Olympus Corporation, Japan). As presented in Fig. 2D, after the excised skins were treated with HP-β-CD-PEI-RhB nanoparticles delivery system for 2 h, strong fluorescence was observed around the pores, indicating that the nanoparticles had traversed the epidermis and penetrated the dermis [38]. At 4 h, the fibers and connective tissue demonstrated obvious fluorescence, indicating penetration of the subcutaneous tissue. Merging the fluores-

cent images allowed direct comparison of the drug (green) and nanoparticle carrier (red). At 2 h, the complete overlap was observed, demonstrating that most of the drug-loaded nanoparticles remain intact in the epidermis and dermis. At 4 h, only the partial overlap was observed that indicates partial disintegration of the nanoparticle drug delivery system during the transdermal process. Until 24 h, we found that stronger red fluorescence appeared and green fluorescence intensity decreased. At 48 h, a few overlap areas could be found and red fluorescence significantly strengthened (Figs. S1 and S2 in Supporting information). This may be due to the drug NaFl was released from the carrier and absorbed, resulting in the green fluorescence decreased. The nanoparticle carriers appearing in red intend to accumulate in the dermis, which further strengthened red fluorescence intensity [39].

In vivo fluorescence images were obtained from depilated Sprague Dawley rats. Specific skin regions were treated with PEI, HP-β-CD, and HP-β-CD-PEI-RhB/NaFl nanoparticle delivery system for 24 and 48 h, respectively. The fluorescent distribution of the drug was determined using an *in vivo* imaging system of IVIS Lumina Series III (PerkinElmer, USA). Regions transdermally administered PEI and HP-β-CD group at 24 h (Fig. 2E) were easily observed that the fluorescence barely diffused, where a small range of fluorescent distribution and the low depth of penetration was presented. In contrast, with nanoparticle administration, the fluorescence was distributed throughout most of the body. The range was mainly focused on the abdominal cavity and backside. That is due to non-specific accumulation and clearance of the nanoparticles in the livers and kidneys, which had been widely reported [40,41]. This was also confirmed by the observation of strong fluorescence intensity in excised livers and kidneys. At 48 h, the distribution areas and fluorescence intensities in the PEI, HP-β-CD slightly increased. The strong fluorescence still focused on the administration region with little diffusion, however, the HP-β-CD-PEI-RhB nanoparticle exhibited a wide area of penetration, and the fluorescence in the administration region significantly diffused around. Finally, only weak blue fluorescent could be observed in the skin region treated. These results demonstrate that the HP-β-CD-PEI-RhB/NaFl nanoparticle delivery system acts as a transcutaneous enhancer, with excellent skin permeation ability and systemic distribution.

To further examine nanoparticle accumulation in the body, sections from different organs (heart, liver, spleen, lung, and kidney) and muscles were observed and quantified using a fluorescence microscope. As presented in Figs. S3 and S4 (Supporting information), the liver and kidney exhibited significant fluorescence signals. This result is in accordance with fluorescent images of IVIS, which indicates that the nanoparticles intend to accumulate in the liver and kidney. Besides, at 48 h, the fluorescence was obviously weakened in the main organs than at 24 h. This suggests that the nanoparticles are mainly metabolized by the liver and spleen. These significant accumulations of different organs also indicate that the HP-β-CD-PEI-RhB/NaFl nanoparticle delivery system can efficiently traverse the skin and delivery drugs to blood circulation.

Compared with the Draize skin irritancy test, the red pigment analysis method can be used to quantify stimulus responses and avoid the subjective influences of individuals during visual observation. Therefore, we used a skin pigmentation analyzer (SPA 99, Courage + Khazakaelectronic GmbH, Cologne, Germany) to measure skin irritation *in vivo* after the application of HP-β-CD, PEI, and HP-β-CD-PEI-RhB nanoparticles on the skin of rabbits. According to the technical guidelines for chemical drug irritation, irritability, and hemolytic activity, rabbits were used as an animal model for skin irritation tests, and 10% (w/v) sodium dodecyl sulfate (SDS) was used as a positive control. After applying SDS and HP-β-CD-PEI-RhB nanoparticles to the rabbit skin, the red pigment index increased significantly (Fig. S5 in Supporting information), indicating that the skin has a strong responsibility to chemical irritants. The red pigment index was highest after SDS treatment and did not decrease during the course of the experiment, indicating irreversible damage to the skin. In contrast, after HP-β-CD-PEI-RhB nanoparticles treatment, changes in red pigmentation were not significantly different with NS and had completely recovered after 24 h. This demonstrates that the nanoparticle causes minimal and reversible skin irritation, and the biosafety of this enhancer in the application of transdermal drug delivery system was better revealed.

Although it has been confirmed that HP-β-CD-PEI-RhB/NaFl nanoparticle delivery system has excellent transdermal penetration effects, its internal mechanism is still unclear. As we all know, transdermal effects are significantly associated with the membrane potential of keratinocytes, and large membrane potential changes can lead to structural changes in the membrane and intercellular space [42]. He *et al.* reported that the cationic *N*-trimethyl chitosan greatly enhanced transdermal penetration by decreasing the membrane potential of HaCaT cells [11]. To investigate whether the HP-β-CD-PEI-RhB/NaFl nanoparticle delivery system could affect membrane potential, we measured the membrane potential of HaCaT cells using a bis-(1,3-dibutyl barbituric acid)-trimethine oxonol ($DiBAC_4(3)$) fluorescent probe. As an anionic dye, $DiBAC_4(3)$ easily enters depolarized cells, while in polarized cells, repulsive interactions hinder its entry [43]. Compared to NS, the fluorescence intensity of HP-β-CD-PEI-RhB/NaFl nanoparticles significantly strengthened (Figs. 3A and B), while the intensity of HP-β-CD was lowest. As a stronger $DiBAC_4(3)$ intensity indicates a lower membrane potential, this suggests that HP-β-CD-PEI-RhB/NaFl nanoparticle delivery system could greatly decrease the membrane potential of HaCaT cells to increase transdermal effects. Interestingly, PEI and HP-β-CD-PEI-RhB nanoparticle both caused decreases in membrane potential, while HP-β-CD did not. Consistent with our previous work [26], this suggests that the effects of the nanoparticle can be mainly attributed to PEI, whose cationic nature induces cell membrane depolarization and greatly improves membrane permeability.

The intracellular Ca^{2+}concentration is significantly associated with membrane potential and fluidity [44,45]. Increased Ca^{2+} can disturb intercellular tight junction distribution and increase barrier function recovery time after skin disruption [46]. After HP-β-CD-PEI-RhB nanoparticle treatment, HaCaT cells were labeled with the fluorescent probe Fluo3-AM to determine the intracellular Ca^{2+}concentration. The fluorescence intensities of the control and HP-β-CD samples were quite low, while they were much higher in the HP-β-CD-PEI-RhB nanoparticle and PEI samples (Figs. 3C and D). Membrane potential depolarization can induce the influx of Ca^{2+}, and the increased intracellular Ca^{2+}concentration can further decrease the membrane potential [47]. Therefore, this result was consistent with a decrease in membrane potential. It also indicates that the HP-β-CD-PEI-RhB nanoparticle can increase the intracellular Ca^{2+} concentration, which can greatly enhance membrane permeability and hinder the barrier function of the skin.

Ca^{2+}-ATPase activity can decrease the intracellular Ca^{2+}concentration by promoting Ca^{2+} efflux, and inhibiting this activity could indirectly increase the intracellular Ca^{2+}concentration [10]. Therefore, Ca^{2+}-ATPase activity was detected using a proprietary kit. Fig. 3E showed that HP-β-CD-PEI-RhB decreased enzyme activity dramatically, by almost a quarter of the activity observed with NS. This suggests that the nanoparticles can decrease Ca^{2+}-ATPase activity, thereby increasing the intracellular Ca^{2+} concentration, which was in accordance with the result of the fluorescent probe Fluo3-AM. Elevated Ca^{2+} concentrations in human keratinocytes can loosen intercellular spaces and increase skin permeability, increasing the transdermal penetration of drugs [42]. Thus, we conclude that HP-β-CD-PEI-RhB nanoparticles can reduce the membrane potential by decreasing Ca^{2+}-ATPase activity

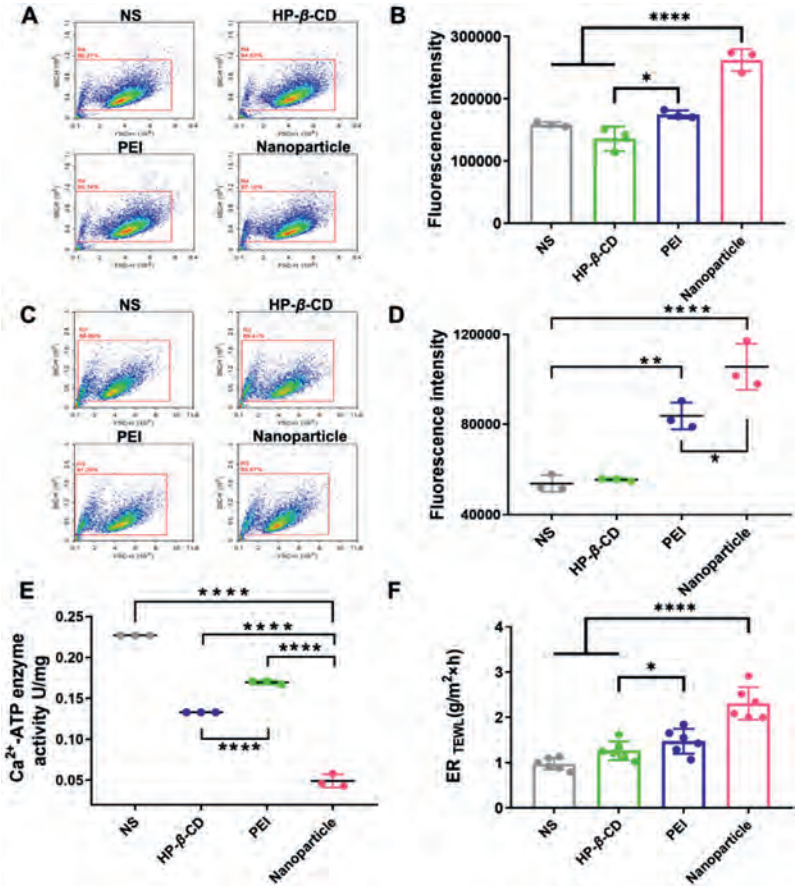

Fig. 3. HaCaT cell membrane potential treated with NS, HP-β-CD, PEI and nanoparticles. (A) The spectrum of HaCaT membrane potential using flow cytometer ($n = 3$). (B) Fluorescence intensity of HaCaT membrane potential ($n = 3$). (C) The spectrum of Ca^{2+} concentration using flow cytometer. (D) Fluorescence intensity of intracellular Ca^{2+} ($n = 3$). (E) The Ca^{2+}-ATP enzyme activity of HaCaT cells ($n = 3$). (F) The value of TEWL of the skin ($n = 5$). Data are presented as mean ± SEM, $^{*}P < 0.05$, $^{**}P < 0.01$, $^{***}P < 0.001$ and $^{****}P < 0.0001$.

and inducing an increased intracellular Ca^{2+} concentration, which is greatly contributed to transdermal drug delivery.

Transepidermal water loss (TEWL) is a crucial parameter used to demonstrate epidermal permeability, as it is significantly inversely correlated with the barrier function of keratinocytes [48]. The approved penetration enhancer Azone greatly improves skin permeability by increasing TEWL, which may be associated with Ca^{2+} influx [49,50]. TEWL was significantly higher with HP-β-CD-PEI-RhB nanoparticles than with NS and was slightly increased with HP-β-CD and PEI (Fig. 3F). The low value in the control demonstrates an intact epidermis that functioned as a permeability barrier. The value with HP-β-CD-PEI-RhB nanoparticle was approximately twice as high as with NS, indicating disruption of the barrier function of the keratinocyte layer. This may also be related to the Ca^{2+} influx induced by the nanoparticles.

Based on the above results, we conclude that nanoparticle-induced Ca^{2+} influx increases the intracellular Ca^{2+} concentration, which can reduce the barrier function of the skin. An imbalance in Ca^{2+} could greatly change the membrane potential, disturbing the arrangement of lipids and cells in the keratinocyte layer and improving the fluidity of the membrane and intracellular spaces, which could greatly increase transdermal drug delivery.

It has been reported that P-gp expresses highly in skin microvascular endothelial cells. To determine whether HP-β-CD-PEI-RhB nanoparticle could modulate dermal P-gp expression, P-gp protein and mRNA expression in HDMECs were performed by using western blotting and qPCR, respectively. Compared to the control, P-gp expression levels have a significant decrease after HP-β-CD-PEI-RhB treatment (Figs. 4A and B). Consistently, P-gp mRNA expression after HP-β-CD-PEI nanoparticle treatment was significantly lower than in the control (Fig. 4C). HP-β-CD and PEI also resulted in decreasing of P-gp expression. These results suggest that the nanoparticles can efficiently decrease P-gp expression of HDMEC cells. This would decrease the drug efflux capability of P-gp, enhancing transdermal absorption.

Next, immunofluorescence staining of P-gp in HDMEC cells was also performed to confirm this result. Verapamil, a well-known P-gp inhibitor [51], was used as a positive control that could reduce the P-gp expression. After co-incubation with HDMEC cells for 48 h, the verapamil group has the weakest fluorescent intensity, suggesting a strong inhibitory effect on P-gp expression. Likewise, the P-gp expression of the nanoparticle showing in green also significantly decreased (Fig. 4D). The results are consistent with the western blotting and qRT-PCR, indicating that the nanoparticles effectively inhibit P-gp expression. Nanoparticles have been reported to overwhelm multidrug resistance to some extent [52]. Positively charged nanoparticles adhere strongly to the negatively charged cell membrane, resulting in accumulation on the cell membrane, which can improve drug penetration into cells.

In this study, dual-labeled nanoparticle drug delivery system that could systematically and vividly probe the transdermal process was conducted. Adopting fluorescence and *in vivo* imaging, it visually demonstrated that the nanoparticle delivery system could cross through the stratum corneum and accumulated in the dermis. To better understand the mechanism of percutaneous absorption, the surface effect of keratinocyte membrane including the

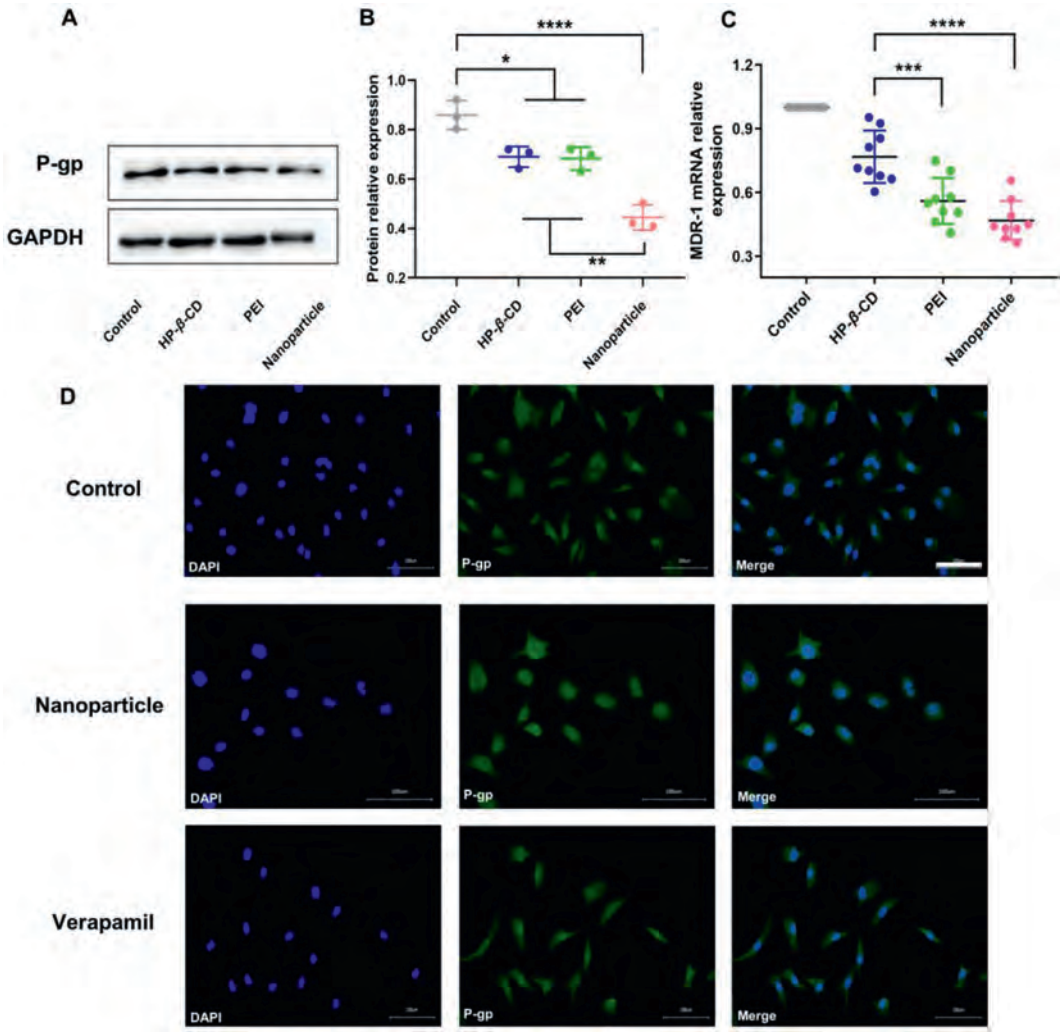

Fig. 4. P-gp expression of HDMEC cells treated with NS, HP-β-CD, PEI, and nanoparticles. (A) Western blot analysis of P-gp expression in HDMEC cells. Verapamil was a positive control ($n = 3$). (B) Quantification analysis of the expression levels of P-gp in HDMEC ($n = 3$). (C) MDR-1 mRNA expression levels of HDMEC cells were analyzed by qRT-PCR ($n = 9$). (D) Immunofluorescent images of P-gp expression ($n = 3$). Cellular nuclei were stained with DAPI (blue). P-gp protein was stained with FITC, appearing in green. Scales bar: 100 μm. Data are presented as mean ± SEM, $^{*}P < 0.05$, $^{**}P < 0.01$, $^{***}P < 0.001$ and $^{****}P < 0.0001$.

membrane potential, Ca^{2+} concentration and Ca^{2+}-ATP enzyme activity were detected, respectively. Herein, we found that the drug delivery system could effectively increase the intracellular concentration of Ca^{2+}, decrease the membrane potential and reversibly regulate TWEL. Besides, the mechanism of P-gp in the skin was also discussed on the level of cellular and molecular biology, containing its relative MDR-1 gene level and protein expression. These results suggest that P-gp expression level is the main factor for transdermal delivery of nanoparticles and by inhabiting the P-gp expression level, and the transdermal effects can be significantly increased. Our work sheds light on the impact of the visualized nanoparticle drug delivery. Simultaneously, we comprehensively and thoroughly discuss the mechanism of the new kind of transdermal drug delivery enhancer *in vitro* and *in vivo*. Basing on the new analytical method for transcutaneous drug delivery, we could deeply learn how to enhance the effect of skin penetration and accelerate the development of TDDS.

Declaration of competing interest

The authors declare that they have no known competing financial interests or personal relationships that could have appeared to influence the work reported in this paper.

Acknowledgments

This work was financially supported by the National Natural Science Foundation of China (No. 81773686), and the Natural Science Foundation of Shaanxi Province, China (Nos. 2021SF-108, 2021SF-308) .

Supplementary materials

Supplementary material associated with this article can be found, in the online version, at doi:10.1016/j.cclet.2021.06.040.

References

[1] H.T.P. Nguyen, E. Munnier, X. Perse, et al., J. Pharm. Sci. 105 (2016) 3191–3198.
[2] M. He, L. Yu, Y. Yang, et al., Chin. Chem. Lett. 31 (2020) 3178–3182.
[3] S. Guo, B. Liu, M. Zhang, et al., Chin. Chem. Lett. 32 (2021) 102–106.
[4] X. Zhou, Y. Hao, L. Yuan, et al., Chin. Chem. Lett. 29 (2018) 1713–1724.
[5] Z. Zhang, P.C. Tsai, T. Ramezanli, B.B. Michniak-Kohn, Wiley Interdiscip. Rev. Nanomed. Nanobiotechnol. 5 (2013) 205–218.
[6] J. Shim, H. Seok Kang, W.S. Park, et al., J. Control. Release 97 (2004) 477–484.
[7] R.S. Nair, A. Morris, N. Billa, C.O. Leong, AAPS PharmSciTech 20 (2019) 69.
[8] M. Chen, G. Quan, Y. Sun, et al., J. Control. Release 325 (2020) 163–175.
[9] M. Kopecna, A. Kovacik, O. Kucera, et al., Mol. Pharm. 16 (2019) 886–897.
[10] S. Ruan, Z. Wang, S. Xiang, et al., Fitoterapia 138 (2019) 104195.
[11] W. He, X. Guo, L. Xiao, M. Feng, Int. J. Pharm. 382 (2009) 234–243.

[12] M.R. Prausnitz, R. Langer, Nat. Biotechnol. 26 (2008) 1261–1268.
[13] J. Chen, Q.D. Jiang, Y.P. Chai, et al., Molecules 21 (2016) 1709.
[14] B.W. BARRY, Int. J. Cosmetic Sci. 10 (1988) 281–293.
[15] T.W. Prow, J.E. Grice, L.L. Lin, et al., Adv. Drug Del. Rev. 63 (2011) 470–491.
[16] Z.L. Chen, T.L. Shi, L. Zhang, et al., Cancer Lett. 370 (2016) 153–164.
[17] J. Sui, M. He, Y. Yang, et al., ACS Appl. Mater. Interfaces 12 (2020) 51198–51211.
[18] M.M. Gottesman, T. Fojo, S.E. Bates, Nat. Rev. Cancer 2 (2002) 48–58.
[19] N. Hashimoto, N. Nakamichi, E. Yamazaki, et al., Int. J. Pharm. 521 (2017) 365–373.
[20] N. Hashimoto, N. Nakamichi, S. Uwafuji, et al., J. Control. Release 165 (2013) 54–61.
[21] D.V. Giacone, V.F.M. Carvalho, S.K.P. Costa, L.B. Lopes, J. Pharm. Sci. 107 (2018) 698–705.
[22] K. Fujita, Y. Masuo, E. Yamazaki, et al., J. Pharm. Sci. 106 (2017) 2632–2641.
[23] M.R. Depaoli, H. Bischof, E. Eroglu, et al., Pharmacol. Ther. 202 (2019) 98–119.
[24] D. Yue, M. Wang, F. Deng, et al., Chin. Chem. Lett. 29 (2018) 648–656.
[25] Z. Tong, J. Zhou, J. Zhong, et al., ACS Appl. Mater. Interfaces 10 (2018) 20014–20024.
[26] K. Wang, Y. Yan, G. Zhao, et al., Polym. Chem. 5 (2014) 4658–4669.
[27] Y. Yan, J. Xing, W. Xu, et al., Int. J. Pharm. 474 (2014) 182–192.
[28] T. Khuroo, D. Verma, S. Talegaonkar, et al., Int. J. Pharm. 473 (2014) 384–394.
[29] M. Tariq, M.A. Alam, A.T. Singh, et al., Colloids Surf. B: Biointerfaces 128 (2015) 448–456.
[30] M.S. Shahab, M. Rizwanullah, S. Alshehri, S.S. Imam, Int. J. Biol. Macromol. 163 (2020) 2392–2404.
[31] S. Bai, V. Gupta, F. Ahsan, Eur. J. Pharm. Sci. 38 (2009) 165–171.
[32] P. Kakar, Z. Li, Y. Li, Y. Cao, X. Chen, J. Control. Release 319 (2020) 428–437.
[33] V.K. Rai, N. Mishra, K.S. Yadav, N.P. Yadav, J. Control. Release 270 (2018) 203–225.
[34] Q. Lv, A. Yu, Y. Xi, et al., Int. J. Pharm. 372 (2009) 191–198.
[35] J. Mosquera, I. García, L.M. Liz-Marzán, Acc. Chem. Res. 51 (2018) 2305–2313.
[36] J. Gao, X. Zhao, W. Jing, et al., React. Funct. Polym. 154 (2020) 104677.
[37] A. Vedadghavami, C. Zhang, A.G. Bajpayee, Nano Today 34 (2020) 100898.
[38] Y. Wang, R. Xu, W. He, et al., Tissue Eng. Part C: Methods 21 (2015) 932–944.
[39] T. Jiang, T. Wang, T. Li, et al., ACS Nano 12 (2018) 9693–9701.
[40] Y. Zhang, B. Zhang, J. Luo, J. Bai, F. Liu, Int. J. Nanomed. 9 (2013) 33–41.
[41] E. Blanco, H. Shen, M. Ferrari, Nat. Biotechnol. 33 (2015) 941–951.
[42] Y. Lan, J.Y. Wang, Y. Liu, et al., China J. Chin. Mater. Med. 40 (2015) 643–648.
[43] D.S. Adams, M. Levin, Cold Spring Harb. Protoc. 2012 (2012) 459–464.
[44] Z. Sulova, M. Seres, M. Barancik, et al., Gen. Physiol. Biophys. 28 Spec No Focus (2009) F89–F95.
[45] F. Savignan, B. Ballion, M.F. Odessa, et al., J. Biomed. Sci. 11 (2004) 671–682.
[46] M. Denda, S. Fuziwara, K. Inoue, J. Invest. Dermatol. 121 (2003) 362–367.
[47] R. Guinamard, L. Salle, C. Simard, The non-selective monovalent cationic channels TRPM4 and TRPM5, in: M.S. Islam (Ed.), Transient Receptor Potential Channels, Springer-Verlag, Berlin, 2011, pp. 147–171.
[48] J.W. Fluhr, R. Darlenski, Transepidermal water loss (TEWL), in: E. Berardesca, H.I. Maibach, K.P. Wilhelm (Eds.), Non Invasive Diagnostic Techniques in Clinical Dermatology, Springer, Berlin Heidelberg, 2014, pp. 353–356.
[49] Y. Katsuta, T. Iida, K. Hasegawa, S. Inomata, M. Denda, Br. J. Dermatol. 160 (2009) 69–74.
[50] X. Liu, P. Quan, S. Li, et al., J. Control. Release 248 (2017) 33–44.
[51] F. Ahmadi, M. Bahmyari, A. Akbarizadeh, S. Alipour, J. Drug Deliv. Sci. Technol. 53 (2019) 101206.
[52] M.S. Singh, A. Lamprecht, Int. J. Pharm. 478 (2015) 745–752.